LU TP 19-24
June 2019

Fitting the three loop pion mass and decay constant to lattice data

Alexandra Wernersson

Department of Astronomy and Theoretical Physics, Lund University

Bachelor thesis supervised by Johan Bijnens

LUNDS UNIVERSITET

Abstract

We perform a fit to three loop order (NNNLO) in Chiral perturbation theory of the pion mass and decay constant. In particular we investigate if the NNNLO fit is an improvement of the fit to two loop order (NNLO) to lattice QCD data, which was done in a lattice gauge group collaboration [1].

We take several steps to improve our fits, one of them being the inclusion of finite volume corrections. They turn out to significantly improve our fits both with one- and two-loop corrections. We find that the NNNLO terms do not provide a significantly better fit to lattice data than the NNLO ones.

Populärvetenskapligt sammanfattning

Kvantkromodynamik har blivit accepterad som den mest välfungerande teorin för den starka växelverkan. Vid höga energier kan kvarkarna i viss mån ses som fria partiklar och den starka kopplingskonstanten, α_S, blir så pass liten att kvantkromodynamiken kan analyseras med en expansion i α_S, en procedur känd som störningsteori. Denna metod fungerar inte längre vid låga energier då α_S kan närma sig ett och den starka växelverkan kan inte längre behandlas som en störning. Andra metoder måste användas om en vill bestämma hadroners massor och andra förutsägelser från kvantkromodynamiken.

Kiral störningsräkning och gitter kvantkromodynamik är två metoder som ofta används tillsammans vid låga energi analyser av kvantkromodynamik. Kiral störningsräkning är en effektiv fältteori, vilket innebär att bara de frihetsgrader som är relevanta vid låga energier behandlas medan de som syns vid högre energier, som till exempel de tre tyngsta kvarkarna, försummas. Gitter kvantkromodynamik är, som namnet avslöjar, kvantkromodynamik på ett gitter istället för i kontinuum. Gittret simuleras på en dator och bland annat hadroners massor kan erhållas. För att spara tid och pengar brukar kvarkarna som simuleras på gittret ha högre massor än vad som hittas i verkligheten. Kiral störningsräkning fungerar då som en bro mellan gittret och kontinuum och de verkliga fysikaliska värdena kan erhållas. Detta fungerar så länge som massorna i gittret sätts till de låga massområdena där kiral störningsräkning är tillämplig. Ett högre massområde kan utnyttjas om en högre ordning av expansionen i kiral störningsräkning läggs till. Hitills har det visat sig att tredje ordningen ger en tydlig förbättring av resultaten vid kiral störningsräkning. Nyligen har fjärde ordningen konstruerats i Lund och frågan är om fjärde ordningen ger ett stort bidrag till resultaten från kiralstörningsräkning eller om de helt kan försummas. Vi undersöker fjärde ordningens bidrag med hjälp av resultat från gitter beräkningar i [1] och även olika sätt att förbättra resultaten från gittret och kiral störningsräkning.

Contents

1 Introduction

In 1960, before Quantum Chromodynamics (QCD) was discovered, an interesting property of the strong interaction was found by Yoichiro Nambu. He proposed that there existed an approximate but hidden symmetry that could explain why some hadrons were lighter than the others. His idea was hard to comprehend until the debut of QCD, a theory in which approximate symmetries are a natural consequence of the quarks coming in different flavours. For the strong interaction, the only difference between the quarks are their masses and since the difference between the lightest quark masses is small, QCD is said to have an approximate symmetry [4].

When approaching higher energies in QCD the strong coupling constant decreases, a phenomenon referred to as asymptotic freedom or perturbative QCD. At higher energies (or smaller distances) the strong interaction can be treated as a perturbation and the theory can be expanded in terms of the strong coupling constant, such a procedure is known as perturbation theory. At low energies however the strong coupling constant is of order unity, making perturbation an unreliable tool for calculating predictions of the QCD lagrangian. To handle the low energy end of QCD one has to restore to other methods.

Chiral perturbation theory (ChPT) and lattice QCD are useful implements for a low energy analysis of QCD. ChPT is an effective field theory meaning that it only uses the degrees of freedom necessary to make calculations at the scale of interest and disregards the ones too heavy to be produced. Lattice QCD on the other hand is merely QCD discretized to a lattice. One of the advantages is that simulations of the lattice can be done on a computer and the hadronic spectrum and matrix elements of operators can be obtained. When implementing lattice QCD the quark masses are set to values larger than their physical masses. When applying ChPT to lattice QCD the masses need to be close enough to their physical values for ChPT to be useful and one can then extrapolate down to the physical values of the quarks. In that sense ChPT can be seen as a bridge between unphysical lattice computations and the physical quantities. Although lattice QCD is improving and has reached the physical point, ChPT can still be used to asses the validity of the lattice results [3].

In this project we study the pion mass and its decay constant, which is the simplest application of higher orders of ChPT. ChPT provides the expansion of M_π and F_π in terms of the quantities obtained from lattice simulations and the low energy constants (LECs) of the theory. ChPT can thus extract the physical values from the lattice QCD simulations and in return lattice QCD provides a way to determine the LECs of ChPT. The results of ChPT have been shown to be more exact when adding higher orders (loops) and in [1] a fit of the pion mass and decay constant was shown to improve after inclusion of next-to-next-to-leading order (NNLO) terms. Recently in Lund, the NNNLO terms were determined [2] and the purpose of this project is to see whether the NNNLO terms give any significant contribution to the fit of the pion mass and decay constant or if they can be neglected.

2 Chiral Perturbation Theory

2.1 QCD and Chiral symmetry

QCD has proven to be a successful theory at large momentum transfers where perturbation theory can be applied. However, at energies below the QCD scale, $\Lambda_{QCD} \approx 1$ GeV, the hadronic spectrum cannot be found as easily. The problem can be solved by noticing that QCD contains an accidental, global symmetry emerging from the fact that the six quarks can be separated by the Λ_{QCD}

$$\begin{pmatrix} m_u \\ m_d \\ m_s \end{pmatrix} << 1 \text{ GeV} \leq \begin{pmatrix} m_c \\ m_b \\ m_t \end{pmatrix}. \tag{2.1}$$

With (2.1) it appears natural to consider only the light quarks when studying QCD at energies below Λ_{QCD}. Consider the three flavour QCD lagrangian

$$\mathcal{L}_{QCD} = \sum_{q=u,d,s} i\bar{\psi}_q(\gamma^\mu D_\mu - m_q)\psi_q - \frac{1}{2}\text{tr}\{G_{\mu\nu}G^{\mu\nu}\}. \tag{2.2}$$

Where ψ_q is the quark field, m_q is the mass of the quark, $D_\mu = \partial_\mu - ig_s A_\mu$ is the covariant derivative and $G_{\mu\nu}$ the gluon field strength tensor which only contains gluon fields.

In order to relate the lagrangian in (2.2) to the symmetry we split the quark fields into left- and right-handed parts

$$\psi_{L/R} = P_{L/R}\psi. \tag{2.3}$$

The QCD lagrangian acquires the following form:

$$\mathcal{L}_{QCD} = \sum_{q=u,d,s} i\bar{\psi}_{qL}\gamma^\mu D_\mu \psi_{qL} + i\bar{\psi}_{qR}\gamma^\mu D_\mu \psi_{qR} - m_q\bar{\psi}_{qL}\psi_{qR} - m_q\bar{\psi}_{qR}\psi_{qL} - \frac{1}{2}\text{tr}\{G_{\mu\nu}G^{\mu\nu}\}. \tag{2.4}$$

When putting $m_i = 0$ the terms in $\mathcal{L}$ are all diagonal and the lagrangian is invariant under independent left- and right-handed rotation. This symmetry of the QCD lagrangian is known as *chiral symmetry*. We can write this as

$$\psi_L \to U_L\psi_L, \qquad \psi_R \to U_R\psi_R, \qquad \psi_{L/R} = \begin{pmatrix} u_{L/R} \\ d_{L/R} \\ s_{L/R} \end{pmatrix}, \qquad U_L, U_R \in SU(3)_L \times SU(3)_R. \tag{2.5}$$

When the masses of the three lightest quarks are put to zero QCD exhibits a three flavour chiral symmetry and the symmetry group becomes $SU(3)_L \times SU(3)_R$. However, since $m_s \simeq 95$ MeV and $m_d \approx 2m_u \simeq 4.6$ MeV the approximation works best with $m_u = m_d = 0$ and m_s held fixed. This is known as two flavour chiral symmetry and the symmetry group becomes $SU(2)_L \times SU(2)_R$ [5].

2.2 Chiral Perturbation Theory

As the name suggests, ChPT builds upon chiral symmetry. ChPT relies on the *assumption* that the chiral symmetry is spontaneously broken. According to the Goldstone theorem this gives rise to Goldstone bosons, the same number as the number of broken generators. The number of broken generators can be related to the number of flavours, N_f via: $N_f^2 - 1$. In the case of two flavours:

$$SU(2)_L \times SU(2)_R \to SU(2)_V.$$

There are three broken generators meaning there should be three Goldstone-bosons, which are identified as the three pions. Because the symmetry is only approximate the bosons are not massless and are therefore referred to as *pseudo*-Golstone bosons. In the three flavour case there are eight light pseudo-Goldstone bosons identified to be the pions, kaons and the eta. A strong indication that chiral symmetry is indeed broken is that no parity doublets are visible in the hadronic spectrum. There are for example not three particles with a similar mass to the pions but with opposite parity. Hence even in a hypothetical massless world the chiral symmetry is spontaneously broken [4].

As was mentioned in the introduction, ChPT is an effective field theory which uses the relevant degrees of freedom for the energy domain in question. For ChPT the scale of interest is Λ_{QCD} and the mesons are used as degrees of freedom rather than the quarks and gluons. ChPT can then be used to calculate for example hadron masses by expansion in a variable $p < \Lambda_{QCD}$. p is usually the momenta or masses and in the next section we will see how to construct the chiral lagrangian from an expansion in p [3].

2.3 Constructing the chiral lagrangian

The effective chiral lagrangian is expanded in increasing orders of p^2:

$$\mathcal{L}_{eff} = \mathcal{L}_2 + \mathcal{L}_4 + \mathcal{L}_6 + \mathcal{L}_8. \tag{2.6}$$

What do the different $\mathcal{L}_n$ look like? We begin with the lowest order term, $\mathcal{L}_2$. The degrees of freedom are the Goldstone bosons discussed in the previous section. They are put in a matrix $\mathcal{U} \in SU(2)$

$$\mathcal{U} = \exp\left(\frac{i\sqrt{2}}{F}\phi\right). \tag{2.7}$$

Where the field ϕ for N_f=2 is a 2×2 matrix containing the pion fields

$$\phi = \begin{bmatrix} \sqrt{2}\pi^0 & \pi^+ \\ \pi^- & -\sqrt{2}\pi^0 \end{bmatrix}. \tag{2.8}$$

In order to incorporate local chiral symmetry, electromagnetism and the quark masses the *external field method* is applied. External fields v_μ, a_μ, s, p are introduced where the vector, v_μ and the axial vector, a_μ, contribute as p in the expansion whereas the scalar, s, and

pseudoscalar[1], p, provides a way to incorporate the quark masses and contribute as p^2. The external fields are hidden within the field χ and the covariant derivative D_μ

$$D_\mu \mathcal{U} = \partial_\mu \mathcal{U} - i r_\mu \mathcal{U} + i \mathcal{U} l_\mu \qquad \chi = 2B(s + ip) = 2B\mathcal{M}. \tag{2.9}$$

where

$$r_\mu = v_\mu + a_\mu, \qquad l_\mu = v_\mu - a_\mu \tag{2.10}$$

Now we can understand why the effective chiral lagrangian has to start at order p^2. At order p^0 there could be no derivatives included and because $\mathcal{U}$ is unitary, $\mathcal{L}_0$ would just be a constant. Lorentz invariance requires an even number of partial derivatives implying that there cannot be an $\mathcal{L}_1$ or any other odd powers of p. We are left with the most general lowest order lagrangian of order p^2

$$\mathcal{L}_2 = \frac{F^2}{4} \langle D_\mu \mathcal{U}^\dagger D^\mu \mathcal{U} + \chi \mathcal{U}^\dagger + \mathcal{U} \chi^\dagger \rangle \tag{2.11}$$

where the trace $\langle ... \rangle$ is over the flavour indices. The lagrangian in (2.11) is associated with the low-energy-constants (LECs) F and B defined as

$$F \equiv F_\pi|_{m_u, m_d \to 0} \qquad B \equiv -\frac{\langle 0|q\bar{q}|0\rangle}{F_\pi^2}\Big|_{m_u, m_d \to 0} \tag{2.12}$$

What is the physical interpretation of F and B? By expanding $\mathcal{U}$ in terms of ϕ an interaction term emerges

$$... - i\sqrt{2} F \langle a_\mu \partial_\mu \phi^\mu \rangle + ... \tag{2.13}$$

The interaction is between the pions contained in ϕ and the external field a_μ, which can be identified as the axial part of the W boson. The interaction vertex of the π^+ decay has coupling constant F. To determine the amplitude of the decay we look at the matrix element between $|\pi^+\rangle$ and the vacuum $\langle 0|$,

$$\langle 0| i\sqrt{2} F \partial_\mu \pi^+ |\pi^+\rangle \equiv i\sqrt{2} F_\pi p^\mu. \tag{2.14}$$

F_π is defined as the decay constant of the pion and the coupling F is its value at the chiral limit ($m_u, m_d \to 0$). Thus (2.14) provides us with a way to measure F at leading order. F_π can also be defined in terms of the matrix elements of the axial current $A_\mu = \bar{d}\gamma_\mu \gamma_5 u$

$$\langle 0|A^\mu|\pi^+\rangle \equiv i\sqrt{2} p^\mu F_\pi e^{-ip\cdot x}. \tag{2.15}$$

$\mathcal{U}^\dagger$ can also be expanded in ϕ, which yields a term containing information about the masses

$$\frac{F^2}{4} \langle -2B\mathcal{M}\phi^2 \rangle \tag{2.16}$$

By evaluating the trace above an expression for the pion mass in terms of the quark masses is obtained

$$M_\pi^2 = 2B\hat{m} \tag{2.17}$$

[1]The use of p for two different quantities is confusing but standard notation in ChPT.

where $\hat{m} = (m_u + m_d)/2$ with $m_u = m_d$. Note however that B is not just any constant of proportionality. In (2.12) we saw that it is related to the *quark condensate* $\langle 0|\bar{q}q|0\rangle$. The fact that $\langle 0|\bar{q}q|0\rangle \neq 0$ is a sufficient way to spontaneously break chiral symmetry. To see why rewrite the quark condensate

$$\langle 0|\bar{u}u|0\rangle + \langle 0|\bar{d}d|0\rangle = \langle 0|\bar{u_L}u_R|0\rangle + \langle 0|\bar{d_L}d_R|0\rangle + \langle 0|\bar{u_R}u_L|0\rangle + \langle 0|\bar{d_R}d_L|0\rangle. \tag{2.18}$$

If the quark condensate experienced a chiral rotation, such that $u_L \leftrightarrow d_L$. The quark condensate becomes,

$$\langle 0|\bar{d_L}u_R|0\rangle + \langle 0|\bar{u_L}d_R|0\rangle + \langle 0|\bar{u_R}d_L|0\rangle + \langle 0|\bar{d_R}u_L|0\rangle \neq \langle 0|\bar{u}u|0\rangle + \langle 0|\bar{d}d|0\rangle \tag{2.19}$$

Hence, by noticing that $\langle 0|\bar{q}q|0\rangle \neq 0$, chiral symmetry is spontaneously broken. B is then a measure of the strength of the symmetry breaking [4].

2.4 Beyond leading order

The next-to-leading order lagrangian, $O(p^4)$, can be constructed in a similar way. Here we only present the form without going into too much detail.

$$\begin{aligned}\mathcal{L}_4 = {} & \ell_1\langle D_\mu\mathcal{U}^\dagger D_\mu\mathcal{U}\rangle^2 + \ell_2\langle D_\mu\mathcal{U}^\dagger D_\nu\mathcal{U}\rangle\langle D^\mu\mathcal{U}^\dagger D^\nu\mathcal{U}\rangle \\ & + \ell_3\langle\chi\mathcal{U}^\dagger\rangle^2 + \ell_4\langle D^\mu\chi D_\mu\mathcal{U}^\dagger\rangle \\ & + \ell_5\langle\mathcal{U}F^{\mu\nu}F_{\mu\nu}\mathcal{U}^\dagger\rangle + \ell_6\langle D^\mu\mathcal{U}F_{\mu\nu}D^\nu\mathcal{U}^\dagger\rangle + \ell_7\langle\tilde{\chi}\mathcal{U}^\dagger\rangle^2\end{aligned} \tag{2.20}$$

where $F_{\mu\nu}$ are operators containing $l_\mu(r_\mu)$. Thus $\mathcal{L}_4$ contains seven additional LECs dependent on a running scale μ, here set to be $\hat{M}_{\pi^+} = 134.8$ MeV. At the higher orders p^6 and p^8 too many LECs for us to write out appear and we instead refer to [8] and [9] respectively. By definition, none of the LECs depend on the u and d masses but may depend on the masses of the other four quarks [1].

When constructing the most general lagrangian of an effective field theory, an infinite number of terms, and thus LECs, emerge. For any given process an infinite number of these terms can contribute. This obviously makes it difficult to make any calculation of a physical observable. The solution is to require a finite accuracy and only include the terms which provide large enough contributions to obtain the desired accuracy. This method of stopping at a certain order in the momentum expansion is known as the *power counting method*. We will discuss the size of the different contributions in the next section [3].

2.5 Renormalization & regularization

In order to understand ChPT a bit better we must introduce a hand-waving explanation of some concepts from quantum field theory. Begin by considering the one-loop diagram in Figure 1. The closed loop contains virtual particles whose momenta can be off-shell and thus do not satisfy the physical constraint $E^2 - p^2 = m^2$. In order to include the

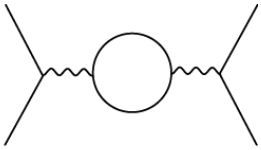

Figure 1: Example of a one-loop diagram.

contribution from the loop, an integration over all possible momenta and space-time has to be done. The integration more often than not leads to infinite contributions from the loop and in order to obtain a finite observable, the contribution has to be removed somehow. The process of removing infinities is known as *renormalization*. When renormalizing a theory, the couplings in the lagrangian have to be redefined such that the loop divergencies are canceled by the tree level ones. Effective field theories such as ChPT are usually non-renormalizable but we will see how ChPT can be renormalizable. The LECs of $\mathcal{L}_4$ are redefined as

$$\ell_i = \ell_i^r + \gamma_i \lambda_0. \tag{2.21}$$

In (2.21) λ_0 contains the counter infinity to the loop ones and the γ_i are constants.

The renormalized LECs, ℓ_i^r, are all finite and depend on the renormalization scale and can be written as

$$\ell_i^r = \frac{\gamma_i}{32\pi}(\bar{\ell}_i + \ln\frac{M_\pi^2}{\mu^2}). \tag{2.22}$$

Where $\bar{\ell}_i$ depend on the scale μ and a logarithmic scale Λ_n

$$\bar{\ell}_n = \ln\frac{\Lambda_n^2}{\hat{M}_{\pi^+}^2}, \qquad n = 1, \ldots, 7. \tag{2.23}$$

Now it is evident that the divergent part is absorbed by the renormalization of the coupling constant at $\mathcal{L}_4$. The loop diagrams should give us a counter contribution to the divergent part in (2.21) in order to make the result finite. The loop integrals can be evaluated using *dimensional regularization*. In short, it consists of evaluating the integrals in $d = 4 - 2\epsilon$ dimensions giving a contribution in expansion of ϵ as

$$\frac{M^2}{16\pi^2}\Big[\lambda_0 - \ln\frac{M^2}{\mu^2}\Big] + \mathcal{O}(\epsilon) \tag{2.24}$$

Where λ_0 in the above equation is the same as the one in eq. (2.21) and $\lambda_0 \propto \frac{1}{\epsilon}$. Since the number of dimensions should be 4 we must take $\epsilon \to 0$ i.e. λ_0 is divergent. Thus when adding the tree level and loop contributions the divergent part in eq. (2.24) and (2.21) will cancel. Important to remember is that a loop diagram must be countered with a tree level diagram of the same order. In this case a p^4 order diagram is countered by a tree level from $\mathcal{L}_4$. ChPT can thus be renormalized by adding the terms of p^n order by order. Furthermore, since p is small, higher order diagrams will give smaller contributions

and one must only calculate the number of diagrams needed to obtain a certain precision. Thus, the inclusion of higher orders might give a better precision but as we saw in section 2.4. higher orders of ChPT comes with more LECs to be determined. One must therefore determine which orders that are necessary to include and which orders to neglect.

A more natural idea, than dimensional regularization, to deal with an integral that diverges at large momentum is to introduce a *cutoff* Λ such that p is contained within $p < \Lambda$. A further improvement of a momentum cutoff is to *discretize* space-time on a lattice such that a field can be associated with a lattice point. This provides a "natural" cutoff when considering the Fourier transform, $\tilde{\phi}(p)$, of a field $\phi(x)$ to momentum space. $\tilde{\phi}(p)$ is periodic, $\tilde{\phi}(p) = \tilde{\phi}(p + \frac{2\pi}{a})$, meaning that the fundamental values of the momentum is contained in the first Brillouin zone, $p \in (-\frac{\pi}{a}, \frac{\pi}{a}]$. When integrating over the momentum a natural momentum cutoff emerges, that is $p < \Lambda = \frac{\pi}{a}$. This regularization method is used in lattice QCD but in general for perturbation theory, dimensional regularization is the one most widely used. We will come back to the discretization of space-time and lattice QCD in section 3.

3 Lattice QCD

3.1 Introduction

Lattice QCD is a non-perturbative implementation applied at low energy scales where perturbation theory cannot be utilized. This means that the masses of the hadrons cannot be calculated with QCD in this energy region even if the quark masses and α_S are known. Lattice QCD is essentially QCD formulated with discretized space-time on a grid (lattice). The new formulation preserves the central elements of QCD like gauge invariance and chiral symmetry. The intention of lattice QCD is to test that QCD is an appropriate theory for the strong interaction also at low energies [10].

The idea of lattice QCD builds upon the evaluation of path integrals. The implementation of path integrals numerically requires several steps, the three considered here are:

- Space-time discretization.
- Construction of the action and the operators.
- The transcription of field variables to the lattice.

3.2 Path integrals

The first two steps are best introduced with an example from quantum mechanics; The transition amplitude for a particle moving from a space-time point (x_0, t_0) to (x_N, t_N) can be determined by evaluating an integral worked out in most quantum mechanics books,

$$\langle x(t)|x(t_0)\rangle = \int_{t_0}^{t} \mathcal{D}x(t) e^{iS[x]} \tag{3.1}$$

where $\mathcal{D}$ is an integral operator and S is the action given by the integral of the lagrangian,

$$S[x] \equiv \int_{t_0}^{t} dt\mathcal{L}(x,\dot{x}) \equiv \int_{t_0}^{t} dt[\frac{m\dot{x}(t)^2}{2} - V(x(t))]. \tag{3.2}$$

The path function in (3.1) is represented by discretizing the time axis into its nodes, $t_j = t_i + ja$ where $j = 1, 2, \ldots, N$ and a is the lattice spacing. For each time interval, the transition amplitude between moving from one space-time point to the other is determined. For example the interval $t_r - t_{r-1}$ corresponds to moving from (x_{r-1}, t_{r-1}) to (x_r, t_r) and the transition amplitude is obtained by integrating over all possible paths, $x_1, x_2, x_3, ..., x_{N-1}$. Then the path integral turns into

$$\int_{t_0}^{t} \mathcal{D}x(t)e^{iS[x]} = \mathrm{A}\int dx_1 dx_2 ... dx_{N-1} e^{iS[x]} \tag{3.3}$$

where A is a normalization constant we will not bother with. In order to evaluate (3.3) the lagrangian has to be discretized so that the action only takes the discrete time points

$$S[x] \equiv \int dt[\frac{m\dot{x}(t)^2}{2} - V(x(t))] \to S[x] = \sum_{j=0}^{N-1}[\frac{m(x_{j+1} - x_j)^2}{2a} + aV(x_j)] \tag{3.4}$$

It is clear from (3.4) that the smaller the a the more exact the discretization will be.

3.3 Lattice QCD

We have constructed the action and the now discretized space-time is associated with points $(x,t) \to (x_i, t_i) = (n_i a, n_t a)$. The quark fields, $\psi(x,t)$, are only described at the sites of the lattice: $\psi(x,t) \to \psi(n_i a, n_t a)$. Next, we have to transcript the gluon fields, A_μ, which mediate the interactions between the quarks. It is somewhat intuitive that if the quark fields are represented on the sites of the lattice then the gluon fields should be found on the links connecting the different sites. The continuum fields $A_\mu(x)$ are replaced by the lattice fields $U_\mu(x)$ fields to conserve gauge invariance on the lattice. The continuum and lattice fields are related via:

$$U_\mu(x) = e^{-iagA_\mu(x)}. \tag{3.5}$$

If $U_\mu(x)$ is a link going from a point x_n to a point x_{n+1} then going in the opposite direction is just the matrix inverse, $U_\mu(x)^{-1}$. Furthermore, since the fields are unitary: $U_\mu(x)^{-1} = U_\mu(x)^\dagger$ and by writing the fields as $U_\mu(x)$, which are generators of SU(3), local gauge invariance is preserved on the lattice. With the $U_\mu(x)$ corresponding to the gluons it is possible to write down a naive, gauge invariant quark action. With the action the path integrals can be evaluated using Monte Carlo methods. The integrals run over all values of the quark and gluon fields (ψ and A) at every point in space-time and are made finite due to the natural momentum cutoff from the discretization, as was mentioned in section 2.5 [10].

Just as with QCD, lattice QCD contains bare quark masses. They emerge as am in lattice units and must be tuned until an accurate hadron mass is obtained. The bare masses are renormalized by multiplicative renormalization constants. Meaning that when the bare mass goes to zero, so does the renormalized one. In order to decrease the computing cost, the quark masses are usually set to higher values than their physical ones. In ChPT $M_\pi^2 \propto m_q$ and the physcial masses can be obtained by extrapolation. Note however that ChPT is only applicable in the small mass region implying that the quark masses will have to be within the region where ChPT works for the theory to give any useful results.

3.4 Errors

The Monte Carlo Method gives rise to the statistical errors. There are also multiple sources of systematic errors which make the results differ from the physical quantities. The main sources of systematic errors are listed below. These are included in the systematic errors quoted in [1].

- **Finite volume** - These errors are due to the fact that simulations are done in finite boxes whereas the calculations are done with infinite lattice spacing. In [12] it has been shown that for large enough L the corrections fall of as e^{-ML}.
- **Fermion doubling** - Fermion doubling is a particular problem that emerges when representing quark fields on a lattice. Without going into too much detail, fermion doubling refers to the fact that when discretizing d dimensions $2^d = 16$ fermions emerges, instead of one, on the edges of the Brillouin zone in the continuum limit $a \to 0$. The solution to this problem in [1] was to introduce *Wilson fermions*. Once again without going into much detail, they emerge by modifying the action such that the additional fermions acquire masses $\propto 1/a$ such that $m \to \infty$ in the continuum limit and does not show up in the array of physical masses.
- **Discretization** - Discretization errors emerge from the fact that $a \neq 0$. Included in this is the error from matching quantities defined in the continuum theory and the lattice equivalents such as quark masses and the axial currents. By investigating the lattice difference, $x_{i+1} - x_i$, with the continuum derivative, it can be shown that the discretization errors grows linearly in a. Reducing a usually takes a great deal of computer cost since the number of lattice points will increase. Therefore, the challenge is to keep the lattice spacing large whilst having small enough discretization errors.

4 ChPT expressions used

4.1 Expressions from lattice paper

In [1] a fit of the pion mass, M_π, and decay constant, F_π, was done to lattice QCD results using $SU(2)$ ChPT. The expansion of M_π and F_π were at the time of the paper known to

NNLO in SU(2) ChPT. The fits were done both in the quark and pion mass expansion, known as x- and ξ-expansion respectively. As in most lattice QCD and ChPT papers the values of the LECs of the studied order of ChPT were determined. The simulations were done with $N_f = 2 + 1$, where N_f is the number of sea quark flavours, the 2 stand for the two lightest quarks with $m_u = m_d$ and the 1 for a heavy strange quark. The ChPT expressions for M_π and F_π at NNLO in the x-expansion are presented below:

$$M_\pi^2 = M^2\Big(1 - \frac{1}{2}x\,\ln\frac{\Lambda_3^2}{M^2} + \frac{17}{8}x^2\left(\ln\frac{\Lambda_M^2}{M^2}\right)^2 + x^2 k_M + O(x^3)\Big)$$

$$F_\pi = F\Big(1 + x\,\ln\frac{\Lambda_4^2}{M^2} - \frac{5}{4}x^2\left(\ln\frac{\Lambda_F^2}{M^2}\right)^2 + x^2 k_F + O(x^3)\Big)$$

$$x = \frac{M^2}{(4\pi F)^2}, \qquad M^2 = 2Bm_{ud}$$

$$B_\pi = \frac{M_\pi^2}{2m_{ud}} \tag{4.6}$$

The $\ln\frac{\Lambda_{M/F}^2}{M^2}$ can be rewritten using the LECs:

$$\ln\frac{\Lambda_M^2}{M^2} = \frac{1}{51}\Big(60\,\ln\frac{\Lambda_{12}^2}{M^2} - 6\,\ln\frac{\Lambda_3^2}{M^2} + 49\Big)$$

$$\ln\frac{\Lambda_F^2}{M^2} = \frac{1}{30}\Big(30\,\ln\frac{\Lambda_{12}^2}{M^2} + 6\,\ln\frac{\Lambda_3^2}{M^2} - 6\,\ln\frac{\Lambda_4^2}{M^2} + 23\Big) \tag{4.7}$$

Where the logarithmic scale Λ_{12} is related to a LEC $\bar{\ell}_{12}$ defined in the same as the ℓ_i in (2.23) and can be written in terms of $\bar{\ell}_1$ and $\bar{\ell}_2$

$$\bar{\ell}_{12} = (7\bar{\ell}_1 + 8\bar{\ell}_2)/15. \tag{4.8}$$

Because the pion mass is related to the quark masses a natural way to expand M_π and F_π is:

$$F = F_\pi\Big(1 - \xi\,\ln\frac{\Lambda_4^2}{M_\pi^2} - 4\xi^2\left(\ln\frac{\Omega_F^2}{M_\pi^2}\right)^2 + \xi^2 c_F + O(x^3)\Big)$$

$$M^2 = M_\pi^2\Big(1 + \frac{1}{2}\xi\,\ln\frac{\Lambda_3^2}{M_\pi^2} + \frac{17}{8}\xi^2\left(\ln\frac{\Omega_M^2}{M_\pi^2}\right)^2 + \xi^2 k_M + O(x^3)\Big)$$

$$\xi = \frac{M_\pi^2}{(4\pi F_\pi)^2} \tag{4.9}$$

Similar to the x-expansion the $\ln\frac{\Omega_{M/F}^2}{M^2}$ can be written in terms of the LECs:

$$\ln\frac{\Omega_M^2}{M_\pi^2} = \frac{1}{15}\Big(60\,\ln\frac{\Lambda_{12}^2}{M_\pi^2} - 33\,\ln\frac{\Lambda_3^2}{M_\pi^2} - 12\,\ln\frac{\Lambda_4^2}{M_\pi^2} + 52\Big)$$

$$\ln\frac{\Omega_F^2}{M_\pi^2} = \frac{1}{3}\Big(-15\,\ln\frac{\Lambda_{12}^2}{M_\pi^2} + 18\,\ln\frac{\Lambda_4^2}{M_\pi^2} - \frac{29}{2}\Big) \tag{4.10}$$

The NLO expressions are simply the above NNLO expressions with the terms containing x^2/ξ^2 omitted.

4.2 Expressions at NNNLO

The expressions at NNNLO are given in [2] and written here:

$$M_\pi^2 = ... + M^2 x^3 \big(a_{30}^M + a_{31}^M L_M + a_{32}^M L_M^2 + a_{33}^M L_M^3\big)$$
$$F_\pi = ... + F x^3 \big(a_{30}^F + a_{31}^F L_M + a_{32}^F L_M^2 + a_{33}^F L_M^3\big) \tag{4.11}$$

for the ξ expansion

$$M^2 = ... + M_\pi^2 \xi^3 \big(b_{30}^M + b_{31}^M L_\pi + b_{32}^M L_\pi^2 + b_{33}^M L_\pi^3\big)$$
$$F = ... + F_\pi^2 \xi^3 \big(b_{30}^F + b_{31}^F L_\pi + b_{32}^F L_\pi^2 + b_{33}^F L_\pi^3\big) \tag{4.12}$$

where $L_M = \log(M^2/\mu^2)$ and $L_\pi = \log(M_\pi^2/\mu^2)$ and '...' are the lower order expansion equivalent to the ones given in (4.6) and (4.9). Some of the parameters were already given in [2]

$$a_{33}^F = -83/24, \quad a_{33}^M = 103/24, \quad b_{33}^F = -5/12, \quad b_{33}^M = 247/48.$$

The parameters with index 32 can be written in terms of the constants

$$\begin{aligned}
a_{32}^F &= \frac{3}{8}\ell_4^q + \frac{27}{2}\ell_2^q + 33\ell_1^q + \frac{1037}{144}, \\
a_{32}^M &= \frac{23}{2}\ell_3^q - 11\ell_2^q - 38\ell_1^q - \frac{91}{24}, \\
b_{32}^F &= -\frac{25}{4}\ell_4^q + \frac{29}{2}\ell_2^q + 16\ell_1^q + \frac{859}{144}, \\
b_{32}^M &= -\frac{1}{2}\ell_4^q - \frac{161}{4}\ell_3^q - 45\ell_2^q - 60\ell_1^q - \frac{71}{3}.
\end{aligned}$$

Where the ℓ_i^q's are related to the renormalized coupling constants ℓ_i^r as, $\ell_i^q = (4\pi)^2 \ell_i^r$. The rest of the a's and b's have too long expressions to be written out here and were always fitted as four free parameters.

4.3 What do we get from the lattice

The lattice paper, [1], includes the fit functions for the x- and ξ-expansion. Below is the fit function for the x-expansion,

$$\frac{(aM_\pi)^2}{2(am_{ud})} = \frac{a^p}{Z_S^p}\Big(1 - \gamma_1^a f(a^p) + \gamma_1^s (\Delta M_{s\bar{s}}^2)^p\Big)(B_\pi^x)(m_{ud}^p; B, F, \dots),$$

$$aF_\pi = \frac{a^p}{Z_A^p}\Big(1 + \gamma_2^s (\Delta M_{s\bar{s}}^2)^p\Big)(F_\pi^x)(m_{ud}^p; B, F, \dots),$$

$$am_{ud} = a^p Z_s^p (1 + \gamma_1^a f(a^p)) m_{ud}^p,$$

$$(aM_{s\bar{s}})^2 = (a^p)^2 (M^p_{s\bar{s}})^2$$
$$a = a^p \qquad Z_A = Z_A^p \qquad Z_S = Z_S^p \tag{4.13}$$

The corresponding fit expression for the ξ expansion is,

$$\frac{2(am_{ud})}{(aM_\pi)^2} = \frac{Z_S^p}{a^p}\Big(1 + \gamma_1^a f(a^p) + \gamma_1^s (\Delta M^2_{s\bar{s}})^p\Big) / B_\pi^\xi(M_\pi^p; B, F, \dots),$$

$$aF_\pi = \frac{a^p}{Z_A^p}\Big(1 + \gamma_2^s (\Delta M^2_{s\bar{s}})^p\Big) F_\pi^\xi(M_\pi^p; B, F, \dots),$$
$$(aM_\pi)^2 = (a^p)^2 (M_\pi^p)^2 \qquad (aM_{s\bar{s}})^2 = (a^p)^2 (M^p_{s\bar{s}})^2$$
$$a = a^p \qquad Z_A = Z_A^p \qquad Z_S = Z_S^p \tag{4.14}$$

where $F_\pi^{x/\xi}$ and $B_\pi^{x/\xi}$ are the ChPT expressions for F_π and B_π at orders NLO, NNLO and NNNLO provided in the previous sections. The quantities necessary to perform the fit are in [1], represented in a large table with 32 values each for: $Z_S \times am_{ud}, aM_{s\bar{s}}, aM_\pi, \frac{aF_\pi}{Z_A}$, as well as their systematic and statistical errors. The lattice QCD simulations in [1] were done at four different values of the coupling constant, g. Each value of g corresponding to one a, Z_A and Z_S. The parameters obtained when fitting the tabulated values in [1] with the ChPT expressions in the previous sections are the LECs, i.e. F, B, $k_{M/F}$, $c_{M/F}$, $\bar{\ell}_i$'s and all the variables with superscript p in the fit functions.

4.4 Understanding the fit functions

Now we will try to make sense of some of the parameters in the above fit equations.

- $f(a^p)$ - In [1] a study was made of discretization errors associated to each lattice quantity. An improvement was only found when adding a^2 corrections to m_{ud} i.e. the $(1 + \gamma_1^a f(a))$. Therefore $f(a) = a^2$ and only added to m_{ud}.

- $\gamma^s_{1/2}(\Delta M^2_{s\bar{s}})^p$ - This parameter is visible in both the M_π and F_π fits. Since the simulations were done at $N_f = 2 + 1$, M_π and F_π experience a small but visible m_s dependence. The $\gamma^s_{1/2}(\Delta M^2_{s\bar{s}})^p$, where

  $$(\Delta M^2_{s\bar{s}}) \equiv (M^2_{s\bar{s}})^p - (M^2_{s\bar{s}})^{\text{ph}} \qquad (M^2_{s\bar{s}})^{\text{ph}} = 685.78\text{MeV [13]} \tag{4.15}$$

  and $(M^2_{s\bar{s}})^p$ found in [1], are included to account for the the strange mass dependence. Note that it would have been equivalent to expand around the strange quark mass, m_s, instead. In [1] it was found that the only order of $\Delta M^2_{s\bar{s}}$ that gave any visible correction was the lowest order (LO). The $M_{s\bar{s}}$ is given by M_π and M_K which to lowest order in ChPT are

  $$M_\pi^2 = B_0(m_u + m_d) \qquad M_K^2 = B_0(m_u + m_s),$$

where B_0 corresponds to B in SU(3) ChPT. The $M_{s\bar{s}}$ is simply

$$M_{s\bar{s}} = 2M_K^2 - M_\pi^2 = 2B_0 m_s. \tag{4.16}$$

The reason for this procedure is that m_s is not directly accessible in the lattice. In [1] this was only done for m_{ud} tabulated under $Z_S \times am_{ud}$. Since M_π was calculated for the fit and M_K had already been obtained in [5], $M_{s\bar{s}}$ is straightforward to obtain from the lattice data.

- Z_S & Z_A - Z_S and Z_A are both renormalization constants. The A in Z_A stands for axial because it is related to the axial current needed for the computation of F_π. The S in Z_S stands for scalar and is needed to convert the bare quark masses to the renormalized masses. Both constants are a way to move from the lattice to the continuum.

- Degrees of freedom (dof) - The lattice paper provides 32 lattice points and to each point corresponds a parameter with superscript p which do not alter the final number of dof. Consider the NLO fit, we have $2 \times 32 = 64$ points to be fitted and the seven fit parameters: $\gamma_1^a, \gamma_1^s, \gamma_2^s, B, F, l_3, l_4$ so the total number of dof is: $64 - 7 = 57$. For the NNLO there are three additional parameters l_{12}, k_F, k_M in the x-expansion and l_{12}, c_M, c_F in the ξ-expansion. For the NNNLO fit there will also be four new parameters, $a^{F/M\prime}s$ and $b^{F/M\prime}s$, if ℓ_{12} is written in terms of ℓ_1 and ℓ_2 or six new since $a_{32}^{F/M}$ and $b_{32}^{F/M}$ are fitted as free if one does not rewrite ℓ_{12}. Thus the higher order of the ChPT expansion, the lower the number of dof. Less degrees of freedom in a fit should give a lower χ^2 and a good quality fit will have $\chi^2 \approx$ dof.

4.5 Finite-volume corrections

An important modification were to add the finite volume corrections when performing the fit, since the chiral calculations in [1] were made with the assumption of an infinite lattice, the finite volume had to be corrected for. In [1] the correction was to one-loop in ChPT but we included one- and two-loops volume corrections. The corrections had already been programmed in [6] in SU(2) ChPT. The relation between the value of each quantity at finite volume and at infinite volume is related to the correction via

$$\Delta F_\pi = F_\pi^V - F_\pi^{V=\infty} \qquad \Delta M_\pi^2 = M_\pi^{2V} - M_\pi^{2V=\infty} \tag{4.17}$$

The finite volume lattice quantities provided in [1] have been corrected for by subtracting Δ from each quantity on the LHS of fits.

The finite volume corrections can be determined using two different methods. The C++ code for both of these were worked out in relation to [6]. The results partly depend on the precision one provides, which should be large enough such that both methods give the same results. Another important point is that ΔM_π^2 must be divided by $2M_\pi$, since the correction is in the squared mass.

5 Fitting the lattice data

We have fitted the lattice data to NLO, NNLO and in the end to NNNLO for F_π and $B_\pi = \frac{M_\pi^2}{2m_u d}$ in the x-expansion and for F_π and B_π^{-1} in the ξ-expansion. The expressions for the x-expansions were straightforward to obtain since the expression for F_π and B_π were simply the ones given in eq. (4.6). The expressions for F_π and B_π^{-1} given by (4.9) required some more thought. The expression for B_π^{-1} is simply $1/B$ times the expression in parenthesis for $\frac{M_\pi^2}{M^2}$, given in (4.9). We saw that ξ depends on F_π meaning that F_π cannot simply be obtained by dividing F by the expression in parenthesis so the expression had to be obtained analytically. By using a little algebra the expression at NNLO can be rewritten as:

$$f(r) \equiv r^4 - r^3 - Cr^2 - D = 0 \tag{5.18}$$

where

$$C = X\ln\Big(\frac{\Lambda_4}{M_\pi}\Big)^2 \qquad D = \frac{X^2}{4}\Big\{\Big[\ln\Big(\frac{\Omega_F}{M_\pi}\Big)\Big]^2 - 4c_F\Big\} \tag{5.19}$$

and

$$r = \frac{F_\pi}{F} \qquad X = \Big(\frac{M_\pi}{4\pi F}\Big)^2 \tag{5.20}$$

Because $D = 0$ at NLO (5.18) reduces to a quadratic equation,

$$r^2 - r - C = 0 \to r = \frac{1}{2}\big(1 \pm \sqrt{1+4C}\big). \tag{5.21}$$

There can only be physical solutions if $C \leq -\frac{1}{4}$ which puts a constraint on the LEC $\bar{l}_4$. Furthermore, the physical solution should have $F_\pi = F$ as $C \to 0$, which gave the final analytic expression for F_π,

$$F_\pi = \frac{F}{2}[1 + \sqrt{1+4C}]. \tag{5.22}$$

At NNLO $f(r)$ is a quartic equation and the derivation for obtaining solutions to a quartic equation will not be derived here. The solutions to a general quartic equation can be found on the Wikipedia page [11]. We present the physical solution for F_π:

$$F_\pi = F\Big\{\frac{1}{4} + S + \frac{1}{2}\sqrt{-4S^2 - 2v + \frac{q}{S}}\Big\} \tag{5.23}$$

where

$$v = -\frac{3}{8} - C \qquad q = \frac{1}{8} + \frac{C}{2} \tag{5.24}$$

and

$$S = \frac{1}{2}\sqrt{-\frac{2}{3}v + \frac{1}{3}\Big(Q + \frac{\Delta_0}{Q}\Big)} \qquad Q = \left[\frac{\Delta_1 + \sqrt{\Delta_1^2 - 4\Delta_0^3}}{2}\right]^{\frac{1}{3}} \tag{5.25}$$

where

$$\Delta_0 = C^2 - 12D \qquad \Delta_1 = -2C^3 - 27D - 72CD. \tag{5.26}$$

The expressions for the NNNLO fit we used are simply the NNLO expressions with the addition of the NNNLO terms given in section 4.2. The analytic expressions in the different expansions were obtained in the same way as in the previous section with F_π in the ξ-expansion being the only exception. We rewrote the NNNLO expression for F as:

$$f(r) \equiv r^6 - r^5 - Cr^4 + Dr^2 + E \tag{5.27}$$

where E is the expression in parenthesis in (4.12) times X^3 (in 5.20). Mathematicians Ruffini, Abel and Galois have proven that equations of degree $n > 4$ posses no algebraic solutions. Therefore, the roots of (5.27) had to be found numerically. We rewrote (5.27) as

$$r = (r^5 + Cr^4 - Dr^2 - E)^{1/6} \tag{5.28}$$

and solved it iteratively in Python, starting at $r = 1$ since $F_\pi = F$ in the zero mass limit.

5.1 χ^2 and error handling

When doing a χ^2 fit the quantity to be minimized is

$$\chi^2(\theta) = \sum_{i=0}^{N} \frac{(y_i - \lambda(x_i, \theta))^2}{\sigma_i^2} \tag{5.29}$$

where the y_i's are the different data points, $\lambda(x_i, \theta)$ is the fit function of data points x_i and parameters θ, the σ_i's are the error corresponding to y_i's. In our fit the lattice points (x_i's) corresponding to the variables with superscript p in (4.13) and (4.14) were are also parameters that needed to be fitted. Thus one further adjustment needs to be explained. In [1] the correlation between the parameters were known and the fully correlated χ^2 fits could be computed

$$\chi^2 = \sum_{i,j} (y_i - \lambda(x_i, \theta)) C_{ij}^{-1} (y_j - \lambda(x_j, \theta)) \tag{5.30}$$

where C_{ij}^{-1} is the inverse of the correlation matrix. Since the lattice quantities obtained in each simulation are correlated, $C_{ij}^{-1} \neq 0$. Instead C_{ij}^{-1} is block diagonal with one large block corresponding to one simulation and the others smaller such that each simulation is almost independent. C_{ij}^{-1} takes into account the correlations between the statistical and systematic uncertainties. This is also the reason for adding the variables with superscript p, correlations in the lattice quantities can be accounted for when computing the χ^2.

Since [1] does not provide the correlation between the quantities, a first guess is to put $C_{ij}^{-1} = \mathbb{1}$. However, since e.g. the $(aM_\pi) = (a^p)(M_\pi^p)$ is correlated with the (aM_π) in $\frac{(2(am_{ud})}{(aM_\pi)^2}$ from (4.14) this lead to missed correlations, especially when performing the ξ fit. Since in [1] the errors, σ_i's, to $\frac{2(am_{ud})}{(aM_\pi)^2}$ and its inverse were known when performing the χ^2 the correlated errors used in [1] are different from our uncorrelated ones. To account for the unknown correlations we instead moved the (aM_π) in 4.14 and the $2(am_{ud})$ in (4.13)

to the RHS of each equation and replaced them by their fitted values. The expressions we used when performing the fits turned into,

$$(aM_\pi)^2 = 2(a^p m_{ud}^p) \times \frac{a^p}{Z_S^p}\Big(1 - \gamma_1^a f(a^p) + \gamma_1^s (\Delta M_{s\bar{s}}^2)^p\Big) B_\pi^x(m_{ud}^p; B, F, \dots), \tag{5.31}$$

$$2(am_{ud}) = (a^p M_\pi^p)^2 \times \frac{Z_S^p}{a^p}\Big(1 + \gamma_1^a f(a^p) + \gamma_1^s (\Delta M_{s\bar{s}}^2)^p\Big) / B_\pi^\xi(M_\pi^p; B, F, \dots). \tag{5.32}$$

Another modification to the fits in (4.14) and (4.13) was to remove the square in $(aM_\pi)^2 = (a^p)^2(M_\pi^p)^2$ and $(aM_{s\bar{s}})^2 = (a^p)^2(M_{s\bar{s}}^p)^2$. This made it easier to find a minimum of χ^2 since at large values of $aM_{\pi/s\bar{s}}$ the square would grow much faster than a linear fit of $aM_{\pi/s\bar{s}}$.

5.2 iMinuit

We performed the χ^2-fit using iMinuit, a robust package for minimizing multi-variable functions. To fit a function through a set of data points the user should provide iMinuit with a χ^2 function between the fit function and the data points and iMinuit will fit the parameters of the function such that the χ^2 is minimized. We wrote functions corresponding to the expressions for F_π in (4.6) and B_π in (4.9) and gave the minimizer a χ^2-function, corresponding to the χ^2 in (5.29), by subtracting the RHS to the LHS in (4.6) and (4.9) including our modifications. iMinuit's minimizer then fitted the variables in order to find a minimum of the χ^2-function. Fitted lattice quantities and parameters were obtained at NLO, NNLO and NNNLO for the x- and ξ-expansion.

6 Results

6.1 Results for χ^2

We present the final χ^2 with and without the inclusion of the finite volume corrections. We fitted M_π and F_π at NNLO and NNNLO with $\bar{\ell}_1$ and $\bar{\ell}_2$ as two free parameters and as one contained in the $\bar{\ell}_{12}$ parameter. Fits have also been done with $\bar{\ell}_{12}$ set to a default value, $\bar{\ell}_{12} = 3.2 \pm 1.2$ in the x-expansion and $\bar{\ell}_{12} = 5.5 \pm 1.5$ in the ξ-expansion, which were the experimental values found in [1]. The result for the x- and ξ-expansions without and with finite volume corrections are tabulated in the Tables below.

Table 1: Results for χ^2 with finite volume corrections from fits in the x-expansion. Once again the fits are to all lattice points and p^4 corresponds to one-loop finite-volume corrections and p^6 to two-loop corrections.

Order	χ^2	χ^2 with p^4	χ^2 with $p^4 + p^6$
NLO	161.2	137.6	120.8
NNLO (Λ_1, Λ_2 free)	55.8	50.9	50.9
NNLO (Λ_{12} free)	55.8	50.9	50.8
NNNLO (Λ_1, Λ_2 free)	52.3	48.5	48.9
NNNLO (Λ_{12} free)	53.0	48.8	49.5
NNNLO (Λ_{12} default)	48.6	48.6	49.5

Table 2: Results for χ^2 with finite volume corrections from fits in the ξ-expansion. Once again the fits are to all lattice points and p^4 corresponds to one-loop finite-volume corrections and p^6 to two-loop corrections.

Order	χ^2	χ^2 with p^4	χ^2 with $p^4 + p^6$
NLO	104.8	88.3	81.9
NNLO ($\bar{\ell}_1, \bar{\ell}_2$ free)	62.6	56.0	55.2
NNLO ($\bar{\ell}_{12}$ free)	62.6	57.7	57.4
NNNLO (ℓ_1, ℓ_2 free)	56.8	51.5	51.9
NNNLO (ℓ_{12} free)	55.2	51.0	51.9
NNNLO ($\bar{\ell}_{12}$ default)	51.8	51.0	51.8

By comparing Table 1, 2 and 3 a clear improvement of χ^2 is seen in the NLO fits when adding finite volume corrections. However, as was mentioned when discussing degrees of freedom, a good fit at NLO should have had $\chi^2 \approx 57$ and even with finite volume corrections the χ^2 for NLO fits are more than two times as large as one would have liked them to be.

The NNLO terms clearly improves the fits by more than halving χ^2 in some cases for both expansions. There is also an evident improvement in χ^2 for all NNLO fits when adding the finite volume corrections. The NNNLO fits shows little improvement over the NNLO ones and although they also improve by inclusion of the finite volume corrections it is not such a noticeable change as with the NLO and NNLO fits. Furthermore, the NNNLO has more parameters that are free to vary so one would have expected the fit to be better since the number of dof were smaller.

By fitting $\bar{\ell}_1$ and $\bar{\ell}_2$ as individual parameters instead of just one parameter, $\bar{\ell}_{12}$, a small improvement was found before adding the volume corrections. One would have expected χ^2 to be higher when putting $\bar{\ell}_{12}$ to a default value since the dof are higher than the other fits at NNNLO. This holds for the χ^2 in Table 1 but once the volume corrections are added this prediction fails and the fits with default $\bar{\ell}_{12}$ experience a better χ^2. It appears as if

a true physical minimum is harder to obtain for the NNNLO fits and therefore it might be that there is a smaller χ^2 for the other NNNLO fits that have not been found. Indeed, the χ^2 obtained from iMinuit becomes more sensitive to the input variables when adding higher orders and this might be why the unexpected results emerge.

Another surprising result for the NNNLO fits is that χ^2 was found to be lower when adding just the p^4 finite-volume corrections than when adding the p^6 finite-volume corrections. There could exist a smaller χ^2 not found but what is more likely is that the NNNLO terms cannot be "seen". Meaning that although the χ^2 is lower, it does not necessarily mean that the NNNLO fits to the lattice quantities are better.

6.2 LECs

In order to say something about the range of applicability for the different ChPT expansions we present the LECs at different M_π^{max} cutoffs. We then compare or values with what was found in [1]. All fits in this section have been done with $\bar{\ell}_{12}$ free.

6.2.1 NLO LECs

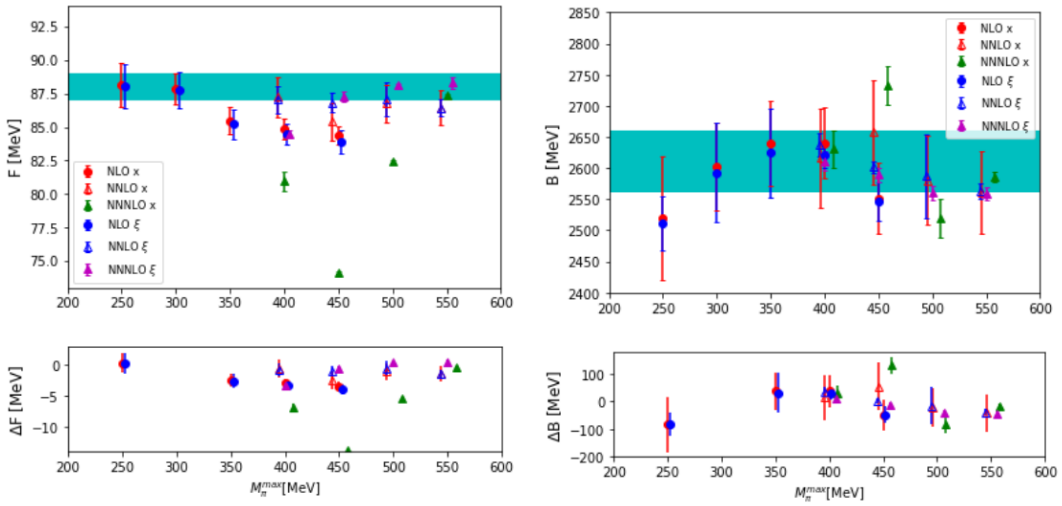

Figure 2: The LECs F and B obtained from fits at different cutoffs. The cyan bar represents the value obtained in [1] with error. We also show the difference of each value to the value obtained at the cutoff $M_\pi^{max} = 300$ MeV, as was done in [1]. The error bars are the statistical errors to the lattice quantities given in [1].

The lower panels in Figure 2 and 3 show the difference of our LECs at different M_π^{max} from $M_\pi^{max} = 300$ MeV, the values are in good agreement with those found in [1]. For the NLO fits the $\Delta F, \ell_3, \ell_4$ in Figures 2 and 3 are all close to zero for $M_\pi^{max} = 250$ MeV and one would have expected the same for ΔB. Nonetheless, at $M_\pi^{max} \geq 350$ MeV the differences becomes several standard deviations from the one at $M_\pi^{max} = 300$ in some cases. We safely

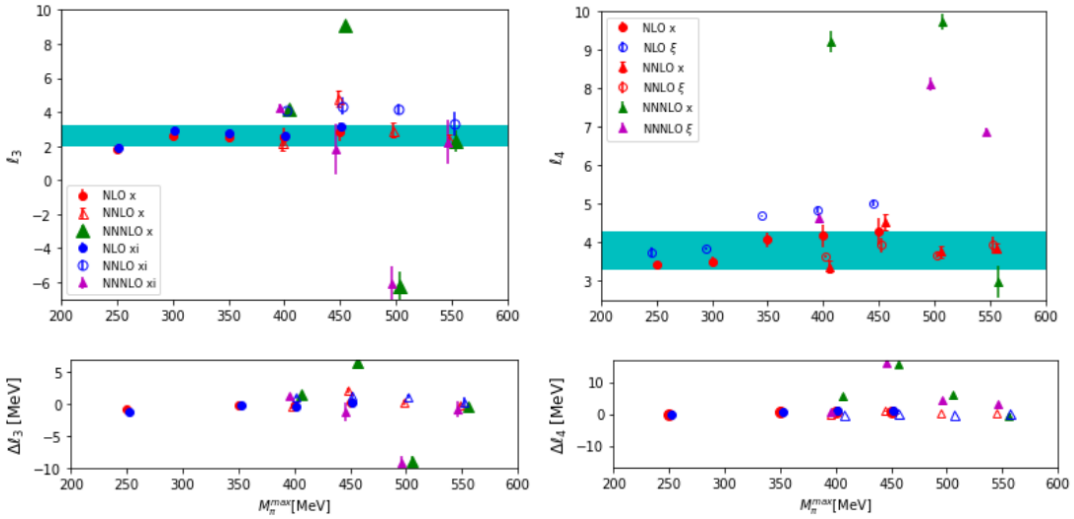

Figure 3: The LECs $\bar{\ell}_3$ and $\bar{\ell}_4$ obtained from fits at different cutoffs. The cyan bar represents the value obtained in [1] with error. We also show the difference of each value to the value obtained at the cutoff $M_\pi^{max} = 300$ MeV, as was done in [1].

conclude that the range of applicability for NLO ChPT does not reach beyond $M_\pi = 300$ MeV which is in agreement with what was found in [1].

The NNLO show a similar trend as the NLO for low M_π^{max}. Therefore, their values are only presented for $M_\pi^{max} \geq 400$ MeV. In [1] the range of applicability for ChPT at NNLO was found to be $M_\pi^{max} = 500$ MeV by an extensive statistical study of the fits, which we have not recreated. However, since our values of the LECs follow a similar trend to what was found in [1] and the deviations from the $M_\pi^{max} = 300$ MeV are in a reasonable range for all cutoffs we suspect that our range of applicability would not reach beyond $M_\pi^{max} = 500$ MeV.

The NNNLO LECs are in clear disagreement with the other two. There are some instances were they agree with the NNLO ones for example at the $M_\pi^{max} = 500$ MeV cutoff but the deviation is often several standard deviations away from the more physical values obtained at NNLO. Note especially how the $\bar{\ell}_4$ at $M_\pi^{max} = 450$ is not visible in the plot of ℓ_4 in Figure 3, it ended up at a value around 20 and had to be cut out in favour of making the other points visible. This is a another example of what was suspected in the previous χ^2 results, that the NNNLO terms do not actually aid in making the fit better.

6.2.2 LECs at NNLO & NNNLO

The values obtained for $\bar{\ell}_{12}$ at NNNLO are mostly in agreement with the ones obtained at NNLO, in Figure 4, considering the errors for this variable. For comparison we also

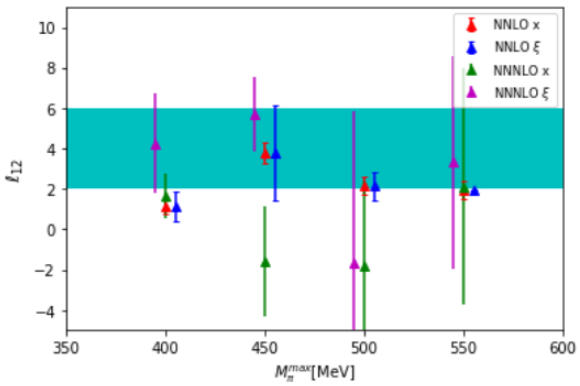

Figure 4: The LECs $\bar{\ell}_{12}$ obtained from fits at different cutoffs. The cyan bar represents the value obtained in [1] with error. We also show the difference of each value to the value obtained at the cutoff $M_\pi^{max} = 300$ MeV, as was done in [1].

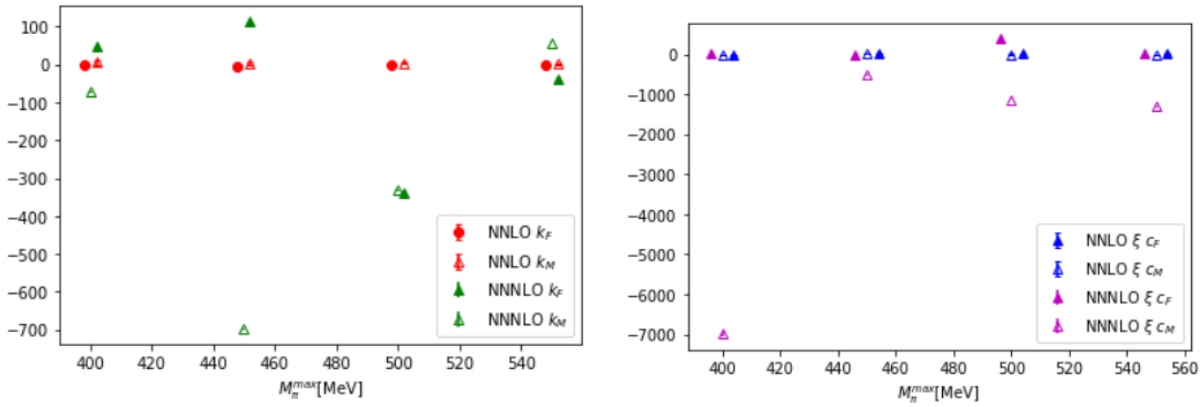

Figure 5: The LECs $k_{M/F}$ and $c_{M/F}$ obtained from fits at different cutoffs in the x- and ξ-expansion respectively.

compute the $\bar{\ell}_{12}$ from the values of $\bar{\ell}_1$ and $\bar{\ell}_2$ obtained in the NNNLO fits where they were left free. We obtain $\bar{\ell}_{12} = -2.6 \pm 13.9$ and $\bar{\ell}_{12} = -6.5 \pm 11.2$ in the x and ξ-expansion respectively, which is in the same range as the values found in [1].

The values for $k_{M/F}$ and $c_{M/F}$ can be found in Figure 5. The values obtained at NNLO are all within the 100 range which is in agreement with what was found in [1]. The values at NNNLO are far away from these and it appears that when fitting a too high order formula to data, the fitted values are often not meaningful, as indicated by the χ^2 not decreasing significantly.

6.3 The chiral fit curves

We present the fit curves from the chiral expansion of M_π and F_π in (4.6) and (4.9) with the parameters obtained from the fit. The fits are the ones for which $\bar{\ell}_{12}$ is left as a free parameter. The curves are plotted with the lattice results for the respective quantity where the discretization and strange mass corrections have been accounted for with the parameters obtained from the fit. These are the multicoloured points corresponding to different β but we have also included the lattice result without any corrections, the yellow points. The lattice spacing is related to the coupling constant g contained in $\beta = \frac{6}{g^2}$.

The curves for the NLO fits in Figure 6 and 7 have been fitted to points with $M_\pi \leq 300$ MeV from the study of the LECs in the previous section. Whereas the curves for the NNLO and NNNLO fits have been fitted to points with $M_\pi \leq 500$ MeV, since we assume that the NNNLO fits do not have a higher range of applicability than the NNLO ones.

By comparing all plots we observe that the NNLO terms clearly improve the fit of the data points. The NLO falls off too soon in the F_π plot and the B_π curve is not as straight as one would have liked it be. The NNLO curve for F_π is almost a straight line through the lattice data points and the curve for B_π is also following the points much better.

We can also consider the yellow points versus the other coloured points. Since the yellow points can be reached from the coloured points by a factor of $\left(1 - \gamma_1^a f(a^p) + \gamma_{1/2}^s (\Delta M_{s\bar{s}}^2)^p\right)$ where parameters are the ones obtained from the fits. The better the fit, the closer should the yellow points be to the other coloured points. By comparing the NLO fits with the NNLO ones it is evident that the discretization and strange mass corrections have improved.

From the plots of the NNNLO fits we see that the fit has not improved much, which could already be guessed by observing how well the NNLO fit the data. The NNNLO curves have acquired more of a bend to accommodate all points. As we have already seen in the previous sections the parameters obtained from the NNNLO fit are usually unphysical. Indeed, when comparing the placement of the yellow points in the NNLO to the NNNLO plots the placement is not better. Some of the points in the NNNLO plots have even moved further away from the other coloured points than in the NNLO plots.

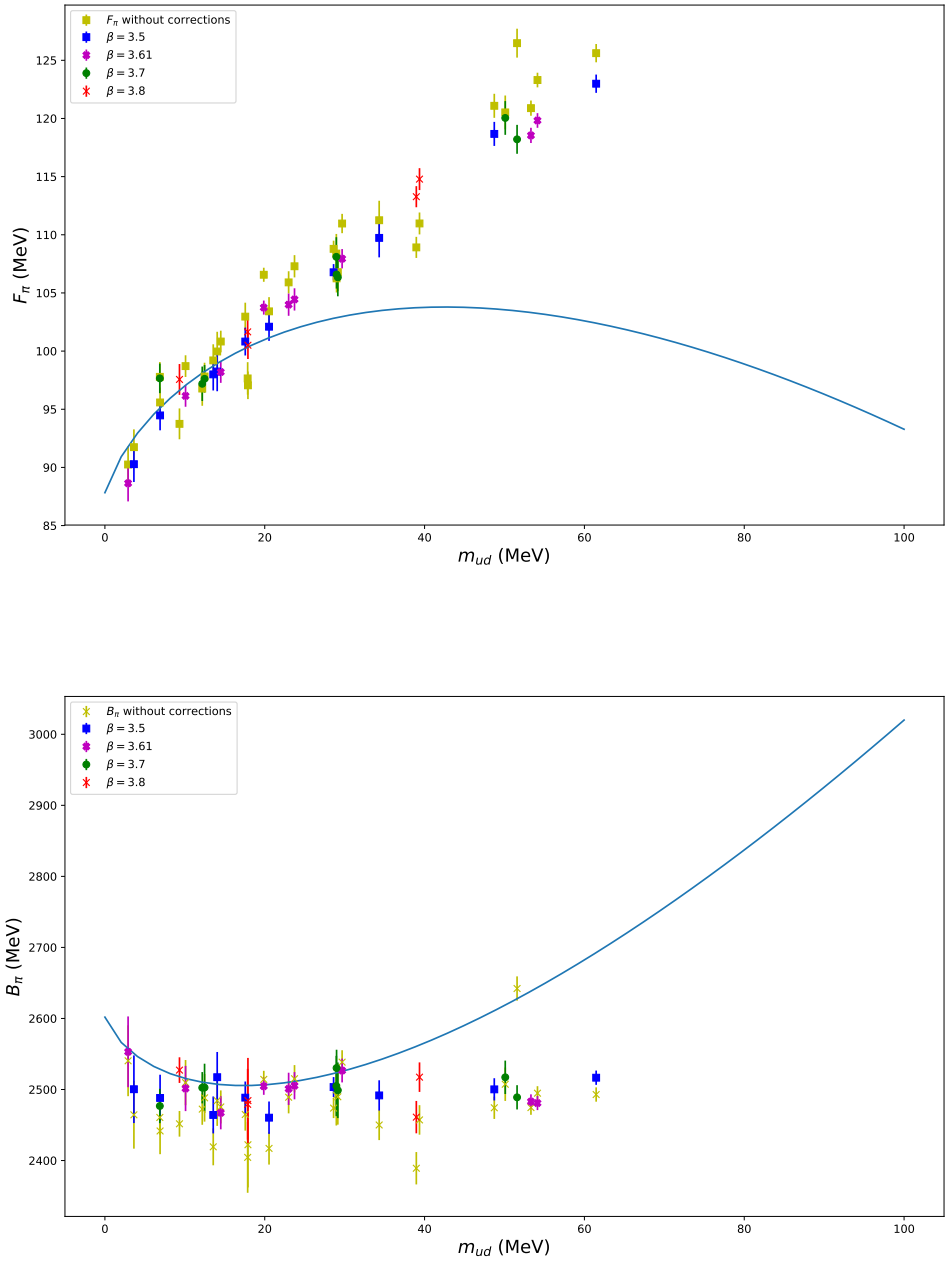

Figure 6: Fits of F_π and B_π to NLO in the x-expansion of points with $M_\pi \leq 300$ MeV corresponding to $m_{ud} \leq 18$ MeV. The yellow points corresponds to the values obtained from the lattice, whereas the other colours correspond to different lattice spacing (β). The error bars are the statistical errors to the lattice quantities given in [1].

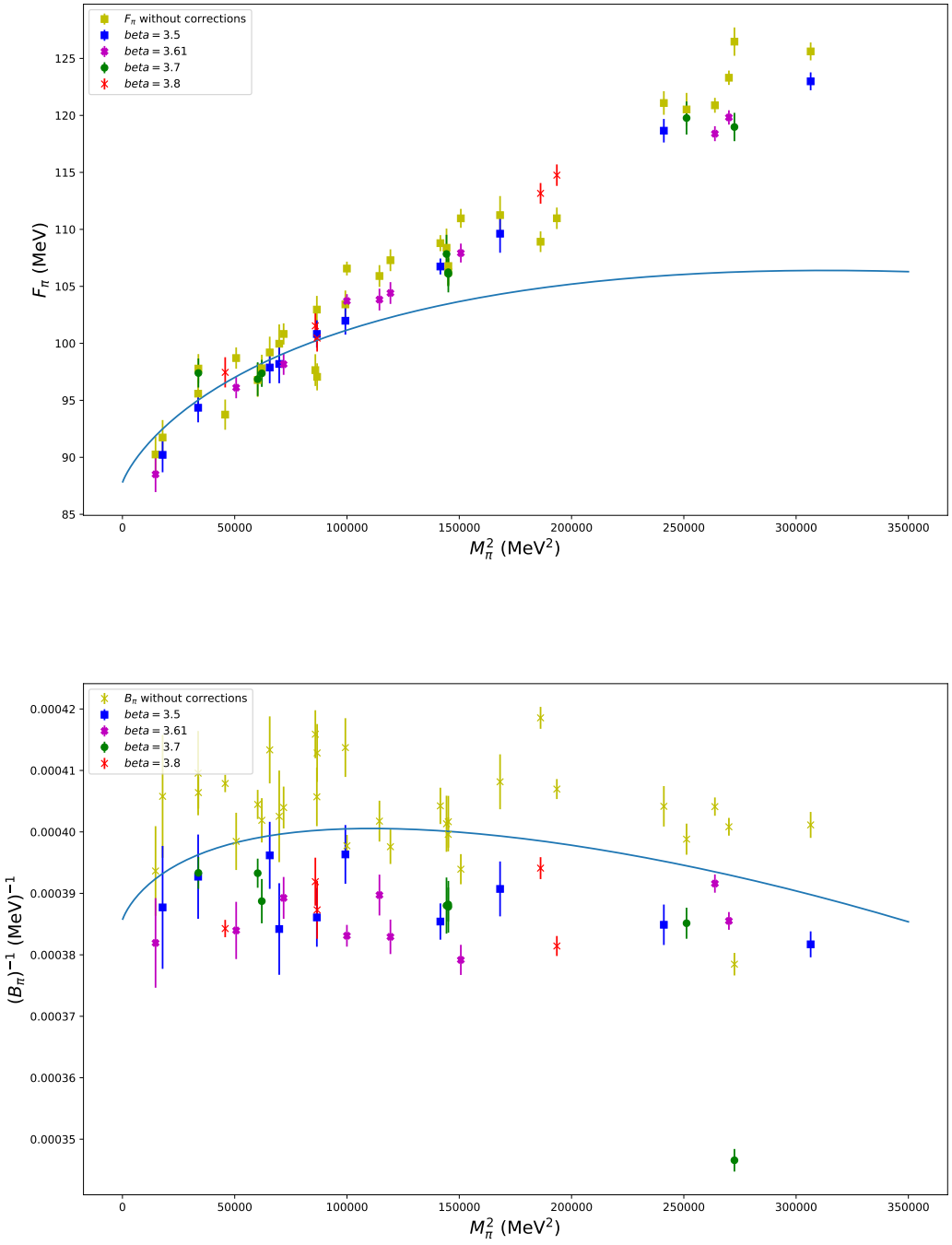

Figure 7: Fits of F_π and $1/B_\pi$ to NLO in the ξ-expansion of points with $M_\pi \leq 300$ MeV corresponding to $m_{ud} \leq 18$ MeV. The description is the same as in Figure 6.

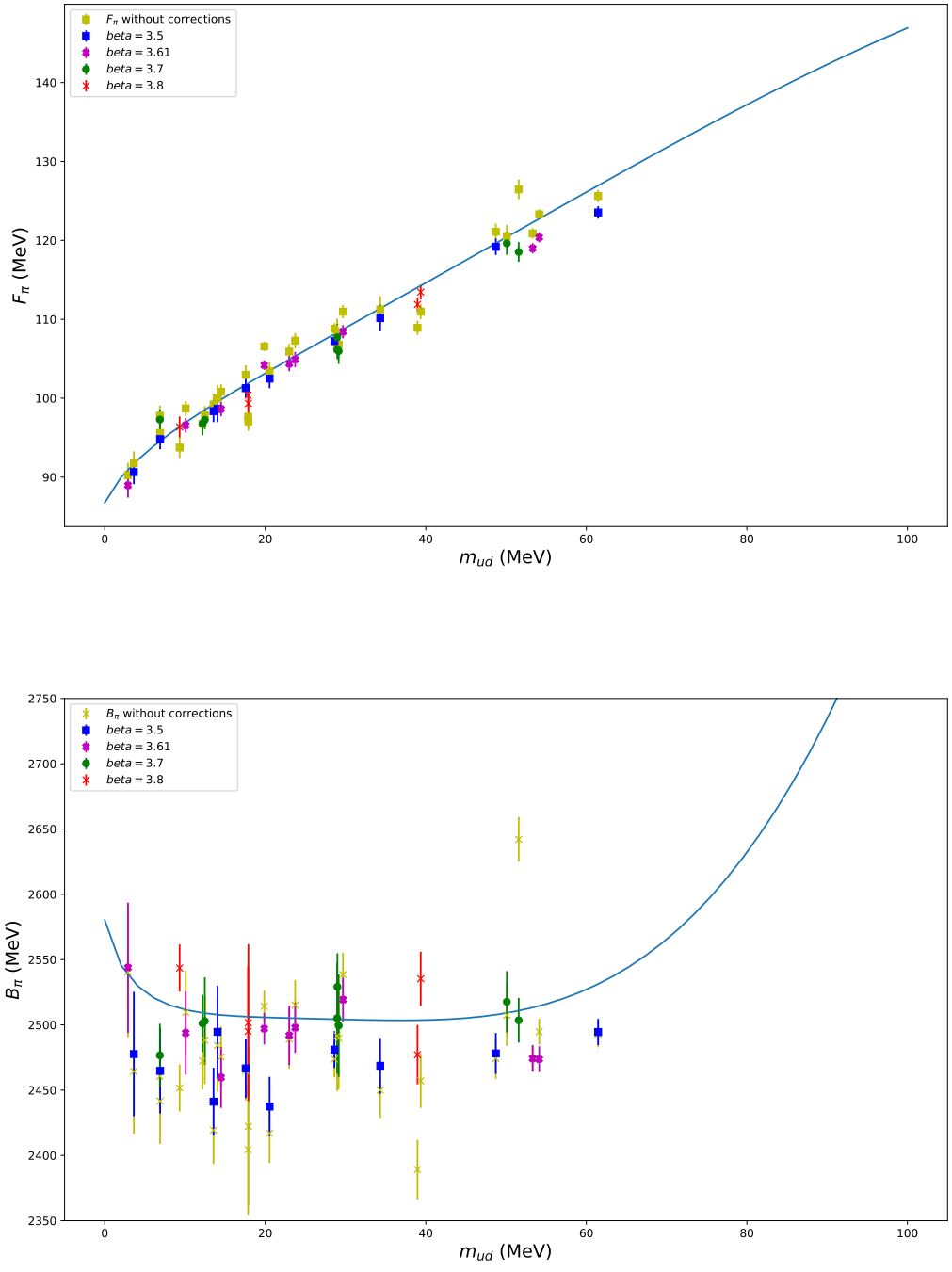

Figure 8: Fits of F_π and B_π to NNLO in the x-expansion of points with $M_\pi \leq 500$ MeV corresponding to $m_{ud} \leq 49$ MeV. The description is the same as in Figure 6.

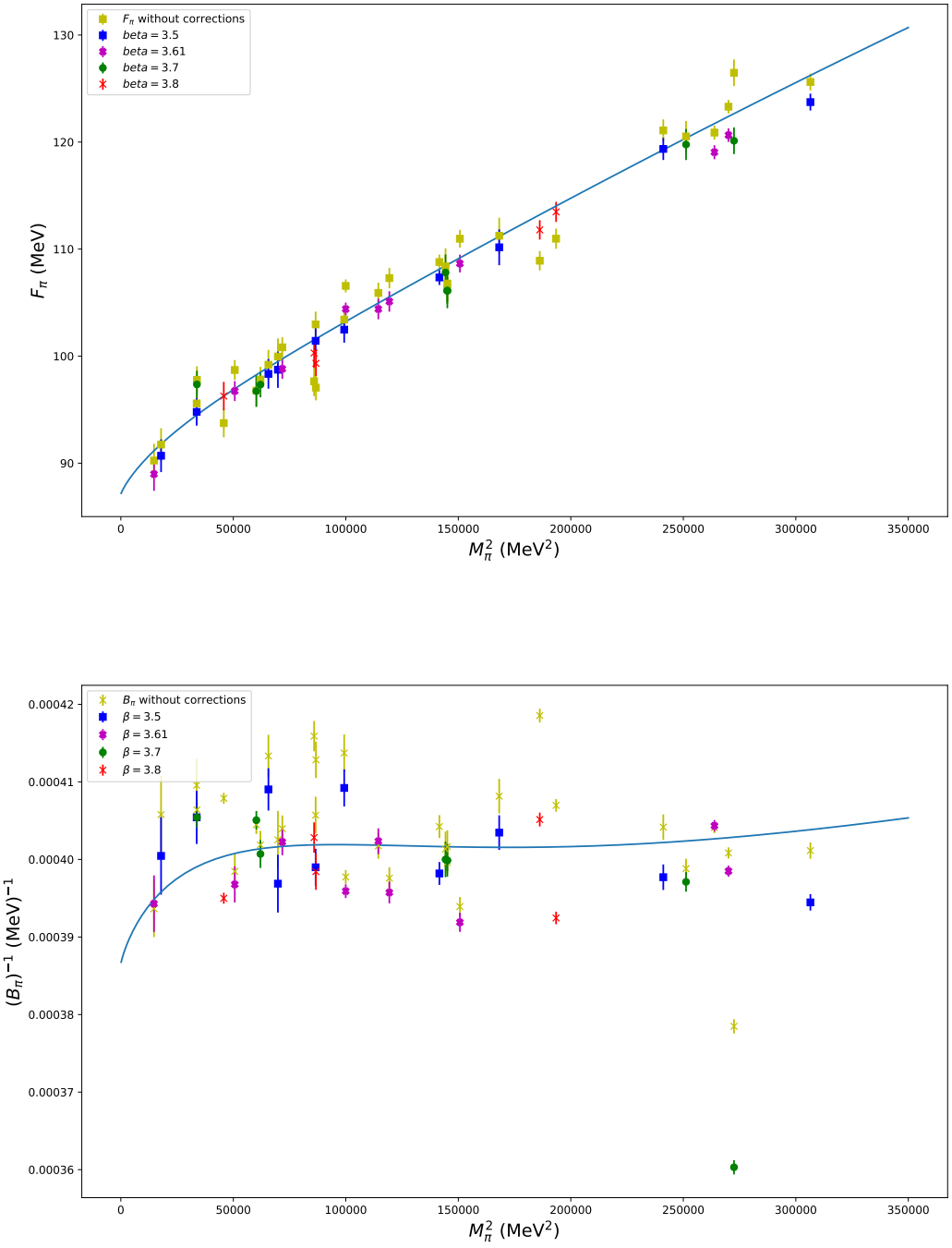

Figure 9: Fits of F_π and $1/B_\pi$ to NNLO in the ξ-expansion of points with $M_\pi \leq 500$ MeV corresponding to $m_{ud} \leq 49$ MeV. The description is the same as in Figure 6.

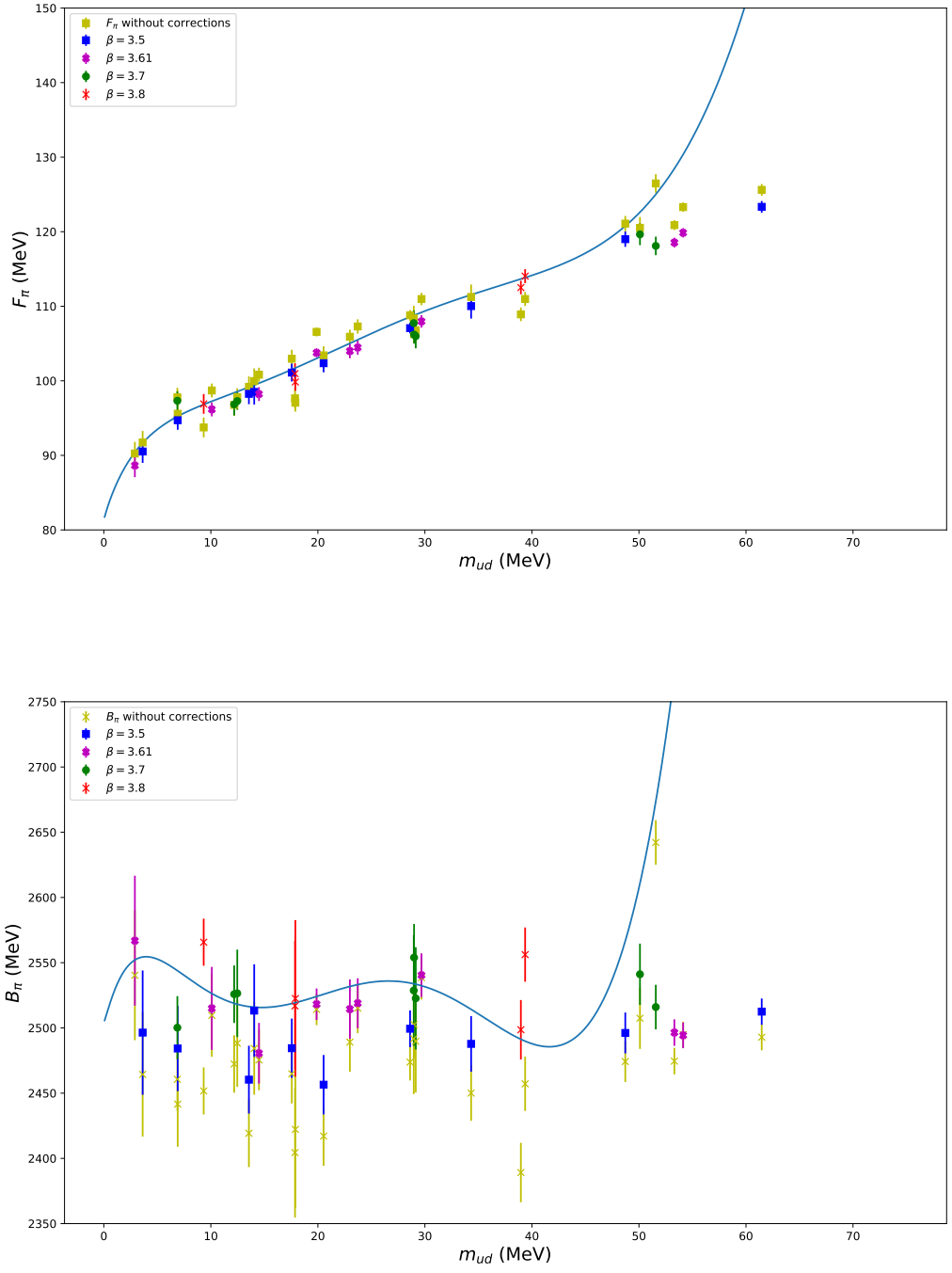

Figure 10: Fits of F_π and B_π to NNNLO in the x-expansion of points with $M_\pi \leq 500$ MeV corresponding to $m_{ud} \leq 49$ MeV. The description is the same as in Figure 6.

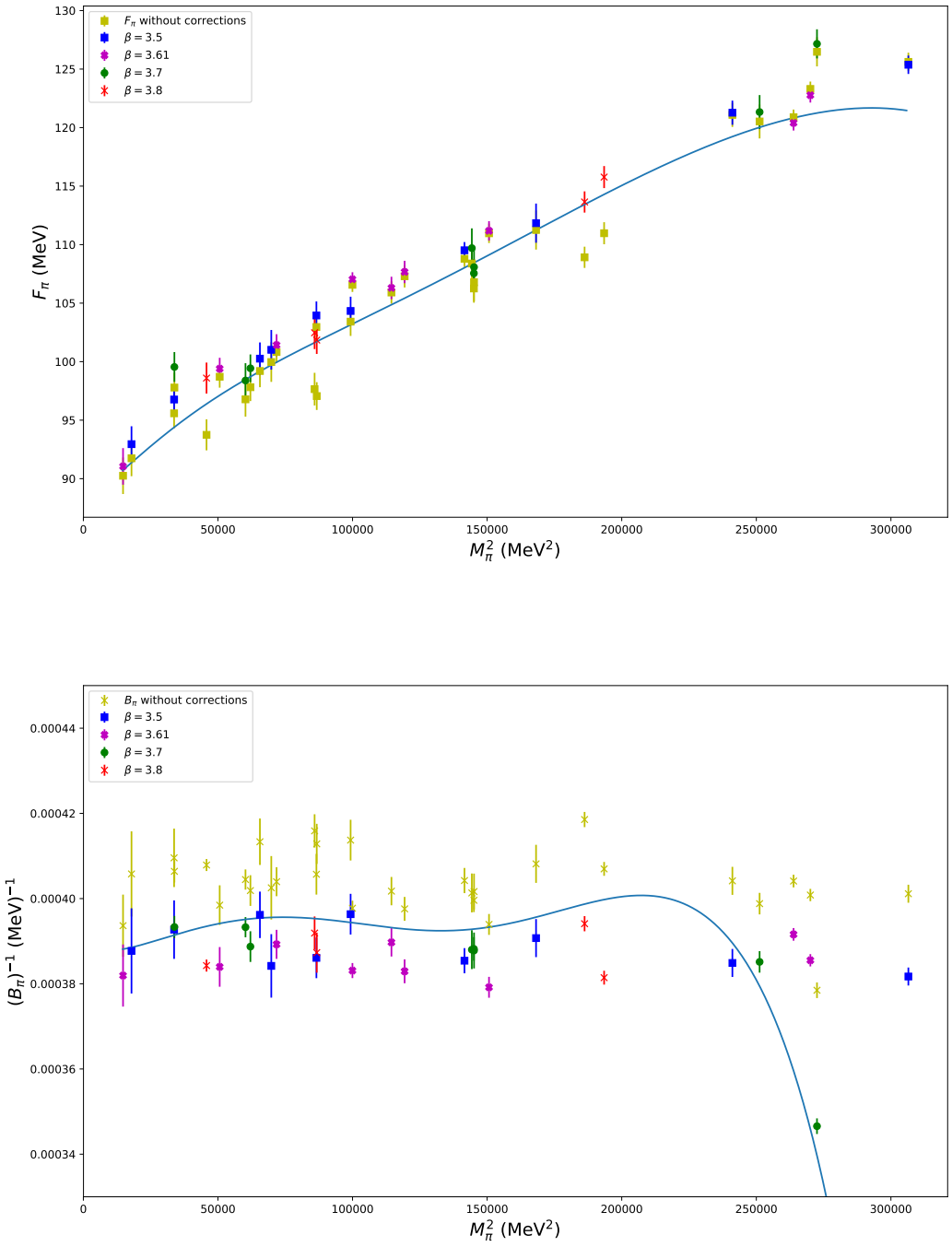

Figure 11: Fits of F_π and $1/B_\pi$ to NNNLO in the ξ-expansion of points with $M_\pi \leq 500$ MeV corresponding to $m_{ud} \leq 49$ MeV. The description is the same as in Figure 6.

7 Conclusions

We have presented fits of F_π and B_π in the x- and ξ-expansions in ChPT to NLO, NNLO and NNNLO. We have shown that NNLO significantly improves the NLO fits whereas the NNNLO fits provide little improvement over the NNLO ones.

We have also found that inclusion of one- and two-loop finite volume corrections significantly improve the fits. An evident improvement was found when including two-loop corrections to the NLO fits and a slight lowering of χ^2 was found in the NNLO ones. We have also found that the NNNLO fits gave the unexpected results of one-loop corrections providing a lower χ^2 than the NNNLO fits with two-loop corrections. We suspect that the "correct" χ^2 is hard to find at this level and that a smaller χ^2 might be possible to obtain.

We have also studied the fits at different M_π^{max} cutoffs and compared the obtained LECs with the ones found in [1]. We found good agreement with [1] at NLO and NNLO but the NNNLO fits resulted in unphysical values at most cutoffs. This was another indication that the NNNLO terms do not serve to improve the NNLO fit but rather fits unphysical values in order to provide a slight lowering of the χ^2.

We have also analyzed our plots of F_π and B_π from our fits. We found once again that the NNLO fit is exceptionally better than the NLO one and our plots are in good agreement with those from [1]. The parameters obtained for the discretization and strange mass corrections are also improved, which is visible in the NNLO plot. We found that the NNNLO plots do not appear to be much better than the NNLO ones which could already be guessed from the previous results.

Although our analysis is thorough a further extension of the project could be to investigate the range of applicability of the different orders. One could for example study the size of the NNNLO terms to the NNLO as a function of mass. To investigate at what point (if at any) the NNNLO contributions might become important. One could also perform a more extensive statistical analysis as was done in [1] to test the quality of the fit and determine whether the inclusion of NNNLO increases the range of applicability of ChPT. Most likely the results found in such analyses would end with the conclusion that the NNNLO terms do not improve the fit much.

Acknowledgements

I would like to thank my supervisor Hans Bijnens for his help and support and for answering all of my questions so thoroughly.

References

[1] **Budapest-Marseille-Wuppertal Collaboration** Collaboration, S. Durr, Z. Fodor, C. Hoelbling, S. Krieg, T. Kurth, L. Lellouch, T. Lippert, R. Malak, T. Metivet, A. Portelli, A. Sastre, and K. Szabo, *Lattice QCD at the physical point*

meets su(2) chiral perturbation theory Phys. Rev. D **90** (Dec, 2014) 114504. http://link.aps.org/doi/10.1103/PhysRevD.90.114504

[2] J. Bijnens N.Hermansson-Truedsson *The Pion Mass and Decay Constant at Three Loops in Two-Flavour Chiral Perturbation Theory* JHEP (2017):181 https://doi.org/10.1007/JHEP11(2017)181

[3] S. Scherer M.R. Schindler *Chiral Perturbation Theory for Mesons. In: A Primer for Chiral Perturbation Theory* (2011) Lecture Notes in Physics, vol 830. Springer, Berlin, Heidelberg https://doi.org/10.1007/JHEP11(2017)181

[4] Heinrich Leutwyler *Chiral perturbation theory.* (2012) Scholarpedia, 7(10):8708. http://www.scholarpedia.org/article/Chiral_perturbation_theory

[5] A.Pich *Chiral Perturbation Theory* (1995) Rep. Prog. Phys. **58** http://ific.uv.es/~pich/Papers/Pich_RPP58_1995_563.pdf

[6] J. Bijnens and T. Rössler, *Finite Volume at Two-loops in Chiral Perturbation Theory*, JHEP **1501** (2015) 034 doi:10.1007/JHEP01(2015)034.

[7] F. James, 1994–1998, CERN Geneva, https://cdsweb.cern.ch/record/2296388/files/minuit.pdf

[8] J. Bijnens, G. Colangelo, G. Ecker *The mesonic chiral lagrangean of order p^6* JHEP 9902, 020 (1999). http://lup.lub.lu.se/record/1890919

[9] J. Bijnens, N.Hermansson-Truedsson, S. Wang, *The order p^8 mesonic chiral Lagrangian* J. High Energ. Phys. (2019):102. https://doi.org/10.1007/JHEP01(2019)102

[10] C. Davies, *Lattice QCD - A guide for people who want results* (2005) Department of Physics and Astronomy, University of Glasgow, UK

https://arxiv.org/pdf/hep-lat/0509046.pdf

[11] *Quartic Function*, (2013) https://en.wikipedia.org/w/index.php?title=Quartic_function&oldid=569041825

[12] M. Lüscher, Selected Topics In Lattice Field Theory, Lectures at the 1988 Les Houches Summer School, North Holland, 1990.

[13] S. Durr, Z. Fodor, C. Hoelbling, S. Katz, S. Krieg, et al., *Lattice QCD at the physical point: simulation and analysis details*, High Energ. Phys. (2011) 2011: 148. doi:10.1007/JHEP08(2011)148.